Composites: Part B 39 (2008) 1196–1204

Contents lists available at ScienceDirect

Composites: Part B

journal homepage: www.elsevier.com/locate/compositesb

Effect of fiber array on damping behaviors of fiber composites

Jia-Lin Tsai *, Yang-Kai Chi

Department of Mechanical Engineering, National Chiao Tung University, Hsinchu 300, Taiwan

ARTICLE INFO

Article history:
Received 21 December 2007
Accepted 7 March 2008
Available online 27 March 2008

Keywords:
B. Microstructures
C. Micromechanics
Fiber array
B. Damping

ABSTRACT

This study aims to investigate the fiber array effect on modal damping behaviors of fiber composites. Three different fiber arrays, i.e., square edge packing (SEP), square diagonal packing (SDP), and hexagonal packing (HP), were considered to represent the microstructures of the unidirectional composites. Repeating unit cells (RUCs) suitable for describing the characteristics of the microstructure were adopted in the generalized method of cell (GMC) micromechanical analysis. The energy dissipation concept was then employed to calculate the specific damping capacities of composites in the material principal directions. The specific damping capacities obtained from micromechanical analysis were regarded as the equivalent damping properties homogenizing in the composites. In conjunction with the modal shapes of the composite structures determined from the finite element analysis, the specific damping capacity was extended to characterize the corresponding modal damping of the composite rods and plates. Both free–free and clamped-free boundary conditions were taken into account in the composite structures. Results indicated that the structures constructed from the composites with SDP fibers exhibit better damping behaviors than the other two cases.

1. Introduction

Fiber composites are basically constructed with fiber and matrix phases. The mechanical behaviors of the fiber composites are always influenced by the fiber and matrix properties and their microstructures such as fiber array, fiber shape, and fiber volume fraction. In order to design composite materials with desired properties, it is required to understand the relation of their microstructure to the overall mechanical responses. The constitutive behaviors of the composites with different fiber architectures have been characterized by many researchers using micromechanical analysis. Zhu and Sun [1] investigated the nonlinear behaviors of AS4/PEEK composites with three different fiber arrays under off-axis loading using finite element approach. It was found that the nonlinear behaviors of the composites were quite sensitive to the fiber packing arrangement. Orozco and Pindera [2] conducted a micromechanical analysis using the GMC model on the two-phase composites with randomly distributed fibers, indicating that, as the number of the refined subcells in the unit cell is increased, the behaviors of the composites tend to be that of a transversely isotropic solid. The influences of fiber shape and fiber distribution on the elastic/inelastic behavior of metal matrix composites were examined by Pindera and Bednarcyk [3] using the GMC micromechanical model. It was revealed that the fiber packing exhibits a substantially greater effect on the responses of the composite materials than does the fiber shape. Tsai and Chi [4] investigated the thermal stress effect on the mechanical behaviors of composites, suggesting that the composites with square edge packing are affected appreciably by the thermal residual stress. A comprehensive review regarding the effect of fiber arrangement on the elastic and inelastic responses of fiber composites was provided by Arnold et al. [5].

Damping is an important parameter in the design of composite materials for engineering applications where dynamic response is concerned and vibration control is required. In order to characterize the damping behaviors of composites, numerous analytical models based on the macromechanical and micromechanical approaches were developed. At macromechanical level, the effect of fiber lay-up sequences on the damping responses were of concern [6,7]. On the other hand, at micromechanical level, most efforts were made on the damping performances associated with the microstructures of fiber composites, such as the fiber volume fraction and the interfacial properties [8–12]. Chandra et al. [8] investigated the shape of fiber cross-section and fiber volume fraction on the damping coefficients of unidirectional composites through the application of viscoelastic correspondence principle. The interfacial properties between the fiber and the surrounding matrix on the damping responses were examined by He and Liu [9] by using the micromechanical model of composite cylinders assembly. In addition, Hwang and Gibson [10] also utilized the finite element approach together with the micromechanical strain energy to predict the fiber–matrix interphase effects on composite damping property. Finegan and Gibson [11] characterized the damping

* Corresponding author. Tel.: +886 3 5731608.
E-mail address: jialin@mail.nctu.edu.tw (J.-L. Tsai).

1359-8368/$ - see front matter © 2008 Elsevier Ltd. All rights reserved.
doi:10.1016/j.compositesb.2008.03.003

behavior of polymer composites with coated fibers, suggesting that the use of a viscoelastic polymer coating on the fiber is an effective way to improve the damping properties. Kaliske and Rothert [12] utilized the damping properties of fiber composites calculated based on the GMC model to derive the structural level damping. Maheri and Adams [13] characterized the modal responses of damped layered composite panels using finite element approach and exhibited good agreements with experimental results. However, in their studies, the microstructure effect of fiber composites on the modal damping responses was not discussed.

In light of the aforementioned investigations, most studies concerned only the fundamental damping behaviors of composite lamina correlated with the fiber and matrix properties. Nevertheless, few investigations focusing on the damping behaviors of the material corresponding to different microstructures were reported. In this study, the effect of fiber arrangement on the basic damping properties of fiber composites was characterized using GMC micromechanical model in conjunction with energy dissipation concept. Subsequently, the fundamental material properties were utilized to construct the overall composites structure. The modal damping responses of the composite structures were then calculated using finite element analysis. The results for the composites structures built based on different fiber array microstructures were compared with each other.

2. Micromechanical approach

2.1. Selection of unit cell

In modeling the mechanical responses of fiber composites using a micromechanical approach, a unit cell needs to be properly selected to represent the microstructures of the materials, and thus, the overall composites responses can be predicted directly from the unit cell. In this study, three different fiber arrays, i.e., square edge packing, square diagonal packing, and hexagonal packing, were considered and illustrated, respectively, in Fig. 1. Based on the periodicity boundary conditions in the uniformly distributed fibers, the repeating unit cells (RUCs) enclosed with dashed lines in Fig. 1 were chosen and utilized to characterize the mechanical properties of the fiber composites associated with different fiber arrangements [14].

2.2. Generalized method of cells

With the ingredient properties and the properly selected RUC, the mechanical behavior of fiber composites can be simulated using the generalized method of cells (GMC) micromechanical model proposed originally by Paley and Aboudi [15]. It is noted that in the GMC analysis, the RUC is usually divided into $N_\beta \times N_\gamma$ subcells as shown in Fig. 2. Based on the displacement continuity on the interface of the adjacent subcells in conjunction with the periodicity condition of the RUC, the relation between overall strain rates and the subcell strain rates is expressed as

$$A_G \eta_s = J\bar{\eta}, \tag{1}$$

where $\eta_s = \{\bar{\eta}^{(11)}, \bar{\eta}^{(12)}, \ldots, \bar{\eta}^{(N_\beta N_\gamma)}\}$ represents the collection of the engineering strain increments for all subcells and $\bar{\eta} = \{\bar{\eta}_{11}, \bar{\eta}_{22}, \bar{\eta}_{33}, 2\bar{\eta}_{23}, 2\bar{\eta}_{13}, 2\bar{\eta}_{12}\}$ indicates the overall strain increments of the RUC. In addition, A_G and J contain geometry parameters of the subcells and the RUC, the dimensions of which are $2(N_\beta + N_\gamma) + N_\beta N_\gamma + 1$ by $6N_\beta N_\gamma$ and $2(N_\beta + N_\gamma) + N_\beta N_\gamma + 1$ by 6, respectively.

In addition, from the traction continuity of the subcells, the relation of subcell strain increment is established as

$$A_M \eta_s = 0, \tag{2}$$

where A_M involves material properties of the subcells. Combining Eqs. (1) and (2) leads to the following expression as

$$\eta_s = A\bar{\eta}. \tag{3}$$

It is noted that A is a $6N_\beta N_\gamma \times 6$ matrix, containing the geometry parameters of the RUC and the material properties of the associated subcells. The A matrix can be further partitioned into the $N_\beta N_\gamma$ entries and each entry represents a 6×6 square matrix as

$$A = \begin{bmatrix} A^{(11)} \\ A^{(12)} \\ \vdots \\ A^{(N_\beta N_\gamma)} \end{bmatrix}. \tag{4}$$

Therefore, the components of the strain increment in the subcells can be expressed explicitly in terms of the overall strain increments as

$$\bar{\eta}^{(\beta\gamma)} = A^{(\beta\gamma)}\bar{\eta}, \tag{5}$$

where $\beta = 1, \ldots, N_\beta$ and $\gamma = 1, \ldots, N_\gamma$.

The constitutive equation of each subcell $(\beta\gamma)$ is written as

$$\bar{\tau}_{ij}^{(\beta\gamma)} = C_{ijkl}^{(\beta\gamma)} \bar{\eta}_{kl}^{(\beta\gamma)}, \tag{6}$$

where $C_{ijkl}^{(\beta\gamma)}$ denotes the elastic stiffness matrix of the subcell $(\beta\gamma)$. It is noted that when the subcells are represented as matrix material, $C^{(\beta\gamma)}$ indicates the stiffness matrix of matrix materials. Whereas, the subcells are denoted as fiber, $C^{(\beta\gamma)}$ becomes the elastic stiffness matrix of the fibers. By substituting Eq. (5) into the subcell constitutive relation given in Eq. (6), the subcell stress components are deduced in terms of the overall strain $\bar{\eta}$ as

$$\bar{\tau}^{(\beta\gamma)} = C^{(\beta\gamma)} A^{(\beta\gamma)} \bar{\eta}. \tag{7}$$

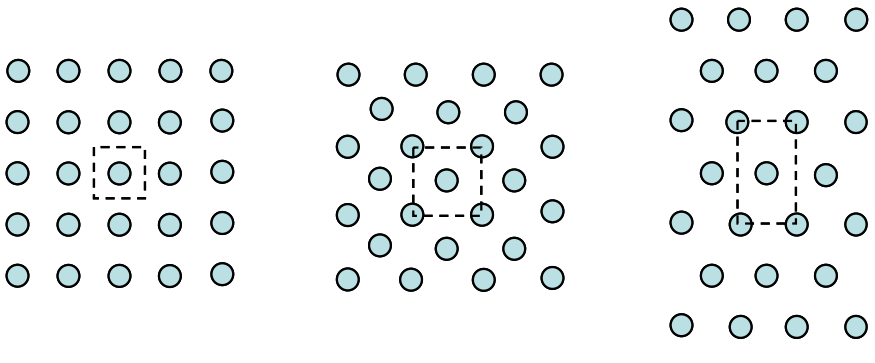

Fig. 1. Three different fiber packing arrangements for fiber composites.

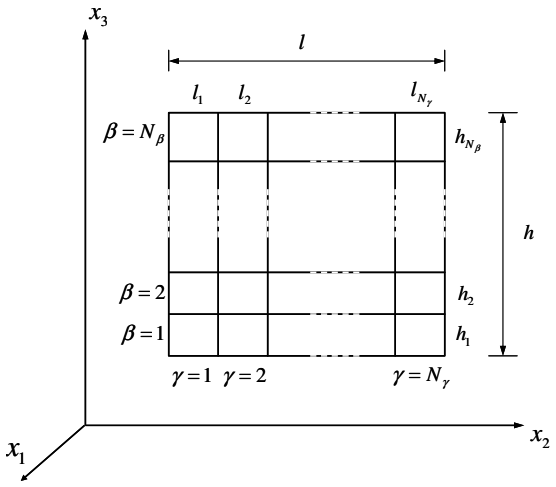

Fig. 2. A typical RUC portioned into $N_\beta \times N_\gamma$ subcells in GMC analysis [15].

Based on the average concept, the overall stress rate of the RUC is written as

$$\bar{\tau} = \frac{1}{hl}\sum_{\beta=1}^{N_\beta}\sum_{\gamma=1}^{N_\gamma} h_\beta l_\gamma \bar{\tau}^{(\beta\gamma)}. \tag{8}$$

With Eqs. (7) and (8), the overall stress rate and strain rate relation of the RUC are established as

$$\bar{\tau} = B^* \bar{\eta}, \tag{9}$$

where

$$B^* = \frac{1}{hl}\sum_{\beta=1}^{N_\beta}\sum_{\gamma=1}^{N_\gamma} h_\beta l_\gamma C^{(\beta\gamma)} A^{(\beta\gamma)}. \tag{10}$$

With ingredient properties as well as RUC geometry, Eq. (10) can be utilized to describe the constitutive behaviors of the composites. When the RUC is applied with a loading $\bar{\tau}$, the corresponding overall strain $\bar{\eta}$ can be calculated from Eq. (9). Afterward, with the assistance of Eqs. (5) and (7), the strain and stress components at each subcell within the RUC can be evaluated.

In the GMC micromechanical analysis, the RUC is divided into the numbers of the subcells representing either fiber or matrix phases. The number of the subcells is dependent on the microstructure of the RUC, including fiber geometry and packing arrangement. In this study, RUC with square edge packing, containing 39×39 subcells as shown in Fig. 3, were employed in the analysis. In addition, the RUCs with square diagonal packing and hexagonal packing were also partitioned into different subcells as shown in Figs. 4 and 5, respectively. It was verified that the present discretizations of RUCs have attained converged results and are suitable for characterizing the mechanical properties of the composites [4].

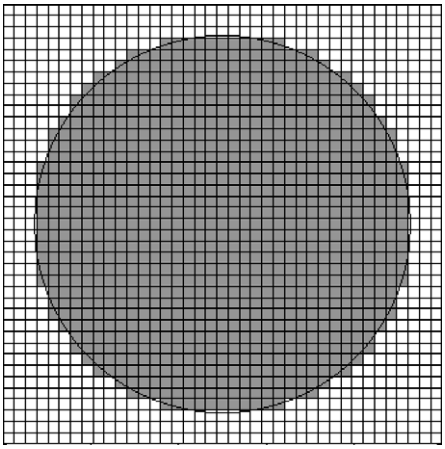

Fig. 3. RUC with square edge packing portioned into 39×39 subcells.

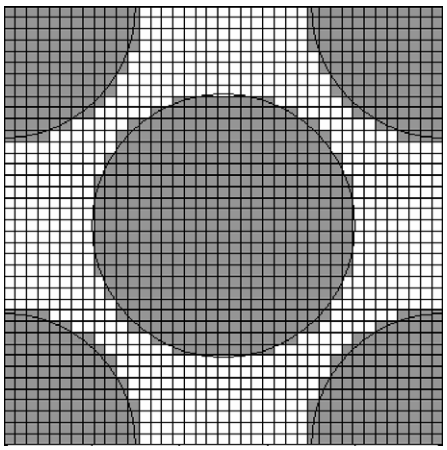

Fig. 4. RUC with square diagonal packing partitioned into 39×39 subcells.

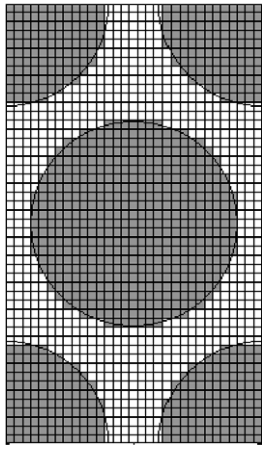

Fig. 5. RUC with hexagonal packing partitioned into 31×49 subcells.

2.3. Calculation of damping capacity of fiber composites

Based on the energy dissipation concept [16], the specific damping capacity of material in vibration was defined as the ratio of the dissipated energy and the stored energy for per circle of vibration

$$\psi = \frac{D}{U}, \tag{11}$$

where D is the energy dissipation per cyclic vibration, and U is the strain energy stored in the material systems when the deformation is maximum. For the fiber composites with fiber and matrix phases, the specific damping capacity given in Eq. (11) can be expressed explicitly in terms of the fiber and matrix parts as

$$\psi = \frac{\psi_f U_f + \psi_m U_m}{U_f + U_m}, \tag{12}$$

where ψ_f is specific damping capacity of the fiber; ψ_m is specific damping capacity of the matrix; U_f indicates strain energy stored in the fiber; and U_m denotes strain energy stored in the matrix. It

is noted that in the above expression, the energy dissipation in the fiber composites assumes to be equal to the summation of the energy dissipations in fiber and matrix phases. In an attempt to evaluate the fundamental damping capacities of fiber composites, the RUC was subjected to an applied loading in material principal directions, and then the stress and strain distributions within the RUC were calculated through the GMC micromechanical analysis. More specifically, a simple loading, such as simple tension, or simple shear in the material principal directions was introduced to the RUC at the beginning. The overall strain $\bar{\eta}$ components can be calculated from the constitutive relation of RUC given in Eq. (9). Subsequently, the corresponding strain and stress components in each subcell were evaluated, respectively, from Eqs. (5) and (7). With the physical quantities, the strain energy in each subcell was calculated as

$$U_{\text{subcell}} = \frac{1}{2}\int_V [\sigma_{11}\varepsilon_{11} + \sigma_{22}\varepsilon_{22} + \sigma_{33}\varepsilon_{33} + \sigma_{23}\gamma_{23} + \sigma_{13}\gamma_{13} + \sigma_{12}\gamma_{12}]\mathrm{d}V. \quad (13)$$

The strain energy in the fiber and matrix phases was determined by summating the energy in the subcells associated with the fiber and matrix domains accordingly. By means of Eq. (12), the damping capacity of the composites can be evaluated from the strain energy of the fiber and matrix as well as their respective damping properties. The isotropic damping properties were assumed in the fiber and matrix phases and the corresponding values are listed in Table 1 [17]. It is noted that for unidirectional composites, because of the attribute of equal properties in the x_2 and x_3 directions (assuming fiber in the x_1-direction), only four independent damping properties (ψ_{11}, ψ_{22}, ψ_{12}, ψ_{23}) are required to be calculated.

The damping property of the unidirectional composites with three different fiber arrangements, i.e., square edge packing, square diagonal packing, and hexagonal packing, obtained from GMC in conjunction with energy dissipation concept are summarized in Tables 2–4, respectively. In the calculation, the fiber volume fraction of composites was assumed to be equal to 60%. For comparison purpose, the finite element analysis was also performed on the RUCs given in Fig. 1. The finite element mesh utilized for the RUC with square diagonal packing is illustrated in Fig. 6. According to the suggestions in the literature [14], the proper boundary conditions for describing the mechanical behavior of the fiber composites were imposed in the RUCs. The damping properties of the RUCs with different fiber arrays evaluated based on the strain energy calculated from FEM analysis were included in the tables. It can be seen that the specific damping capacity obtained from the GMC analysis are quite close to those derived from FEM analysis, except for ψ_{23} properties. The discrepancy could be attributed to the strict constrain conditions, i.e., the interface traction rate continuity, are imposed on the subcell interfacial regions in the GMC model. Such constraint condition causes the stress component σ_{23} calculated in all subcells to be the same when the composites are subjected to a pure shearing [18], and thus, the damping property ψ_{23} calculated based on the GMC model is not relied on the fiber array. However, from the FEM analysis, it was shown the value of ψ_{23} are varied depending on the fiber arrays. As a result, in theory, the ψ_{23} obtained from GMC analysis may not be valid.

Table 1
Mechanical properties and damping capacities of fiber and matrix used in GMC analysis [17]

	Fiber	Matrix
E_1 (GPa)	225	3.197
E_2 (GPa)	15.64	
G_{12} (GPa)	38.03	
G_{23} (GPa)	52.48	
ν_{12}	0.229	0.347
ν_{23}	0.49	
Ψ	0.00101	0.06537

Table 2
Damping property of fiber composites with SEP packing obtained by using the GMC and FEM analysis

SEP	GMC	FEM	Error (%)
ψ_{11}	0.00123	0.00123	0
ψ_{22}	0.01311	0.01256	4.3
ψ_{12}	0.02124	0.02164	1.8
ψ_{23}	0.01793	0.01688	6.2

Table 3
Damping property of fiber composites with SDP packing obtained by using the GMC and FEM analysis

SDP	GMC	FEM	Error (%)
ψ_{11}	0.00123	0.00123	0
ψ_{22}	0.01742	0.01658	5
ψ_{12}	0.02254	0.02175	3.6
ψ_{23}	0.01793	0.01137	57.6

Table 4
Damping property of fiber composites with HP packing obtained by using the GMC and FEM analysis

HP	GMC	FEM	Error (%)
ψ_{11}	0.00123	0.00123	0
ψ_{22}	0.01621	0.01477	9.7
ψ_{12}	0.02236	0.02164	3.3
ψ_{23}	0.01793	0.01444	24.1

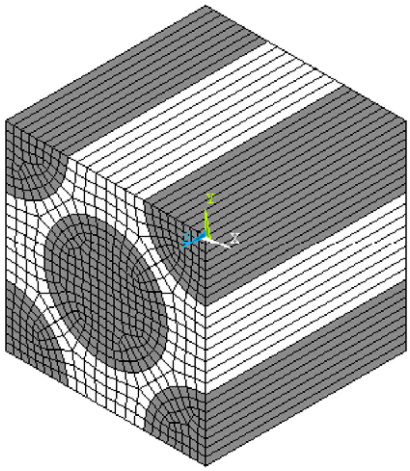

Fig. 6. Finite element mesh of the RUC with square diagonal packing (gray region: fiber, white region: matrix).

3. Determination of modal damping of composite structures

From the GMC analysis together with the energy dissipation concept, we have derived the damping properties of unidirectional composites in the material principal directions. However, when the composite structures are adopted for engineering applications, the vibration in bending and torsional modes generally takes place, and the damping properties associated with these vibration modes have to be characterized accordingly. Here we adopted the two-step simulation procedure to predict the damping behaviors of the composite structures when they are in vibration motions. First,

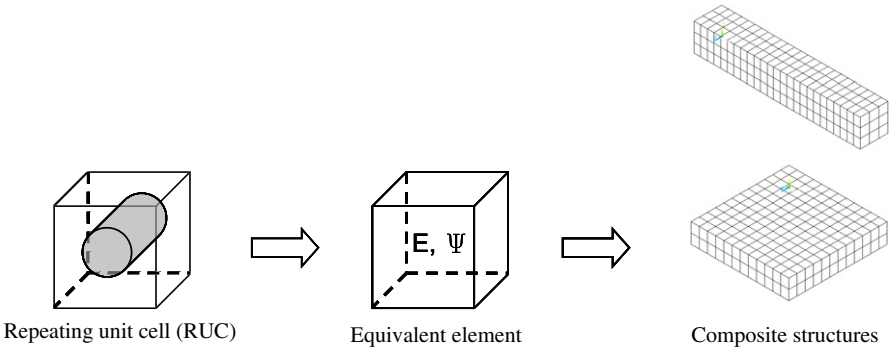

Fig. 7. Modeling procedure for characterizing the damping properties of composite structures.

the basic material properties of the unidirectional composites, such as E_1, ψ_{11}, E_2, ψ_{22}, G_{12}, ψ_{12}, G_{23}, and ψ_{23}, were evaluated using the GMC micromechanical model. Afterwards, the material properties were considered as macromechanical properties of the equivalent volume element, which would be the fundamental building block of composites structures. The detail analytical procedure was illustrated in Fig. 7.

The modal damping capacities of composite structures in bending and torsion vibration modes were derived from the finite element (FEM) analysis together with the strain energy dissipation concept. For a linear elastic material, the strain energy stored in a volume element is expressed as

$$U^{(\text{element})} = \frac{1}{2}\int_V \sigma_{11}\varepsilon_{11} + \sigma_{22}\varepsilon_{22} + \sigma_{33}\varepsilon_{33} + \sigma_{23}\gamma_{23} + \sigma_{13}\gamma_{13} + \sigma_{12}\gamma_{12}\mathrm{d}V = \frac{1}{2}\int_V \{\sigma\}^{\mathrm{T}}\{\varepsilon\}\mathrm{d}V. \tag{14}$$

Substituting the constitutive relation $\{\sigma\} = [C]\{\varepsilon\}$ into Eq. (14) yields

$$U^{(\text{element})} = \frac{1}{2}\int_V \{\varepsilon\}^{\mathrm{T}}[C]\{\varepsilon\}\mathrm{d}V, \tag{15}$$

where $[C]$ is a 6×6 symmetric stiffness matrix of composites. The corresponding dissipated strain energy of the volume element can be written in terms of the specific damping capacity as

$$D^{(\text{element})} = \frac{1}{2}\int_V \psi_{11}\sigma_{11}\varepsilon_{11} + \psi_{22}\sigma_{22}\varepsilon_{22} + \cdots + \psi_{12}\sigma_{12}\gamma_{12}\mathrm{d}V = \frac{1}{2}\int_V \{\sigma\}^{\mathrm{T}}[\psi]\{\varepsilon\}\mathrm{d}V = \frac{1}{2}\int_V \{\varepsilon\}^{\mathrm{T}}[C][\psi]\{\varepsilon\}\mathrm{d}V, \tag{16}$$

where $[\psi]$ indicates the matrix form of damping properties of equivalent elements as

$$\psi = \begin{bmatrix} \psi_{11} & 0 & 0 & 0 & 0 & 0 \\ 0 & \psi_{22} & 0 & 0 & 0 & 0 \\ 0 & 0 & \psi_{22} & 0 & 0 & 0 \\ 0 & 0 & 0 & \psi_{23} & 0 & 0 \\ 0 & 0 & 0 & 0 & \psi_{12} & 0 \\ 0 & 0 & 0 & 0 & 0 & \psi_{12} \end{bmatrix}. \tag{17}$$

Therefore, with the strain energy and the strain energy dissipation given in Eqs. (15) and (16), respectively, the specific damping capacity of a volume element can be written as follows:

$$\psi^{(\text{element})} = \frac{D^{(\text{element})}}{U^{(\text{element})}} = \frac{\frac{1}{2}\int_V \{\varepsilon\}^{\mathrm{T}}[C][\psi]\{\varepsilon\}\mathrm{d}V}{\frac{1}{2}\int_V \{\varepsilon\}^{\mathrm{T}}[C]\{\varepsilon\}\mathrm{d}V}. \tag{18}$$

In the finite element method, the displacement field $\{u\}$ and strain field $\{\varepsilon\}$ in the element can be represented by the nodal displacement as well as the shape function as

$$\{u\} = [N]\{d\}, \tag{19}$$

$$\{\varepsilon\} = [B]\{d\}, \tag{20}$$

where $[N]$ is the shape function; $\{d\}$ is nodal displacement; and $[B]$ is the differentiation of shape function $[N]$.

A combination of Eqs. (18) and (20) leads to

$$\psi^{(\text{element})} = \frac{\frac{1}{2}\int \{d\}^{\mathrm{T}}[B][\psi][C][B]\{d\}\mathrm{d}V}{\frac{1}{2}\int \{d\}^{\mathrm{T}}[B][C][B]\{d\}\mathrm{d}V}. \tag{21}$$

It is noted that in Eq. (21), $\{d\}$ indicates the nodal displacement of a volume element. For a structure vibrating in a certain natural frequency, $\{d\}$ can be regarded as the mode shape of structure, representing the relative nodal displacement of the element.

The mode shape of the composite structure will be evaluated from structural dynamics analysis using finite element approach [19] as shown in the following. The equation of motion for a volume element is written as

$$[m]^{(\mathrm{e})}\{\ddot{d}\} + [k]^{(\mathrm{e})}\{d\} = 0, \tag{22}$$

where the element mass matrix $[m]^{(\mathrm{e})}$, and element stiffness matrix $[k]^{(\mathrm{e})}$ is defined as

$$[m]^{(\mathrm{e})} = \int_V^{(\mathrm{e})} \rho[N]^{\mathrm{T}}[N]\mathrm{d}V \tag{23}$$

$$[k]^{(\mathrm{e})} = \int_V^{(\mathrm{e})} [B]^{\mathrm{T}}[C][B]\mathrm{d}V, \tag{24}$$

where ρ is the density of the material. Substituting Eq. (24) into Eq. (21), the specific damping capacity for a volume element is yielded as

$$\psi^{(\text{element})} = \frac{\frac{1}{2}\{d\}^{\mathrm{T}}[k]_{\psi}^{(\mathrm{e})}\{d\}}{\frac{1}{2}\{d\}^{\mathrm{T}}[k]^{(\mathrm{e})}\{d\}}, \tag{25}$$

where $[k]_{\psi}^{(\mathrm{e})}$ representing the "energy dissipation stiffness matrix" is written as

$$[k]_{\psi}^{(\mathrm{e})} = \int_V^{(\mathrm{e})} [B]^{\mathrm{T}}[C][\psi][B]\mathrm{d}V. \tag{26}$$

For the global structure responses, the structure mass matrix $[M]$ and the structure stiffness matrix $[K]$ can be derived through the superposition of the element mass matrix $[m]^{(\mathrm{e})}$ and stiffness matrix $[k]^{(\mathrm{e})}$ given in Eqs. (23) and (24), respectively, by properly

assigning each element matrix in the structure matrix depending on the structure node numbering. As a result, the equation of motion for the structure can be written as

$$[M]\{\ddot{d}\} + [K]\{d\} = 0. \tag{27}$$

The natural frequency and mode shape of the composites structures associated with each vibration mode can be evaluated by solving the eigenvalue problem of Eq. (27). The eigenvalue and eigenvector $\{\Phi\}$ of Eq. (27), representing the natural frequency and modal shape of the structure, respectively, were calculated by Matlab commercial code with the "eig" command. It is worthy to mention that in the calculation of the mode shape of the composite structures, the effect of material damping was neglected, and only the mass matrix and stiffness matrix were taken into account.

From the definition of specific damping capacity, the modal damping capacity of the structure associated to each modal shape can be expressed in terms of the global stiffness matrix $[K]$, the global energy dissipation stiffness matrix $[K]_\psi$, and the corresponding modal eigenvector $\{\Phi\}$ as

$$\psi_i = \frac{\frac{1}{2}\{\Phi_i\}^{\mathrm{T}}[K]_\psi\{\Phi_i\}}{\frac{1}{2}\{\Phi_i\}^{\mathrm{T}}[K]\{\Phi_i\}}, \tag{28}$$

where the index i indicates the i^{th} modal shape. It is noted that the global energy dissipation stiffness matrix $[K]_\psi$ is obtained from the superposition of the energy dissipation stiffness matrix given in Eq. (26).

4. Results and discussion

In order to investigate the fiber arrangement effect on the modal damping capacity of composite structures, both rod type and plate type structures were taken as examples. Moreover, two different boundary conditions, i.e., free–free and free-clamped boundary conditions, were also considered in this study.

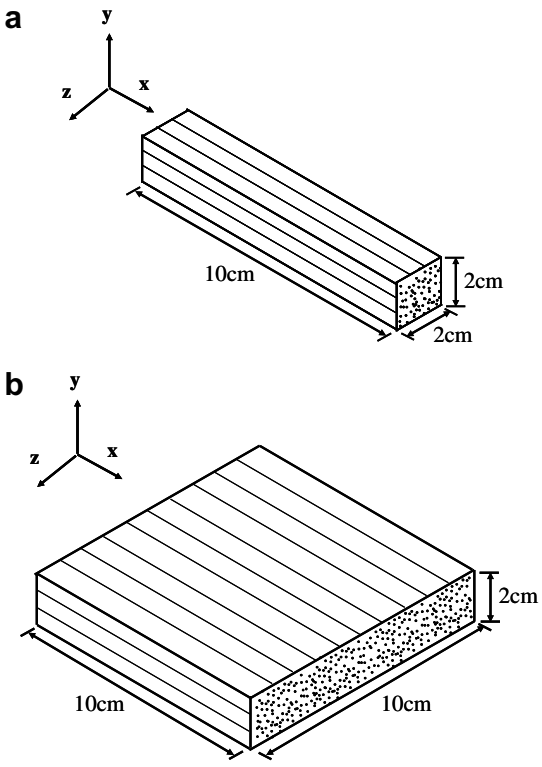

Fig. 8. The dimension of composite structures (a) composite rod (b) composite plate.

4.1. Vibration with free–free boundary condition

The dimensions of the composite structures used in the simulation were illustrated in Fig. 8 where the fiber was extended in the x-direction. Because of the free–free boundary condition, the first six modal shapes were the rigid body motion and eliminated in the following modal analysis. The first three modal shapes of the composite rod are shown in Fig. 9. It is indicated that for the structure configuration, the first mode is torsional mode which is followed by the two bending modes. Table 5 shows the modal

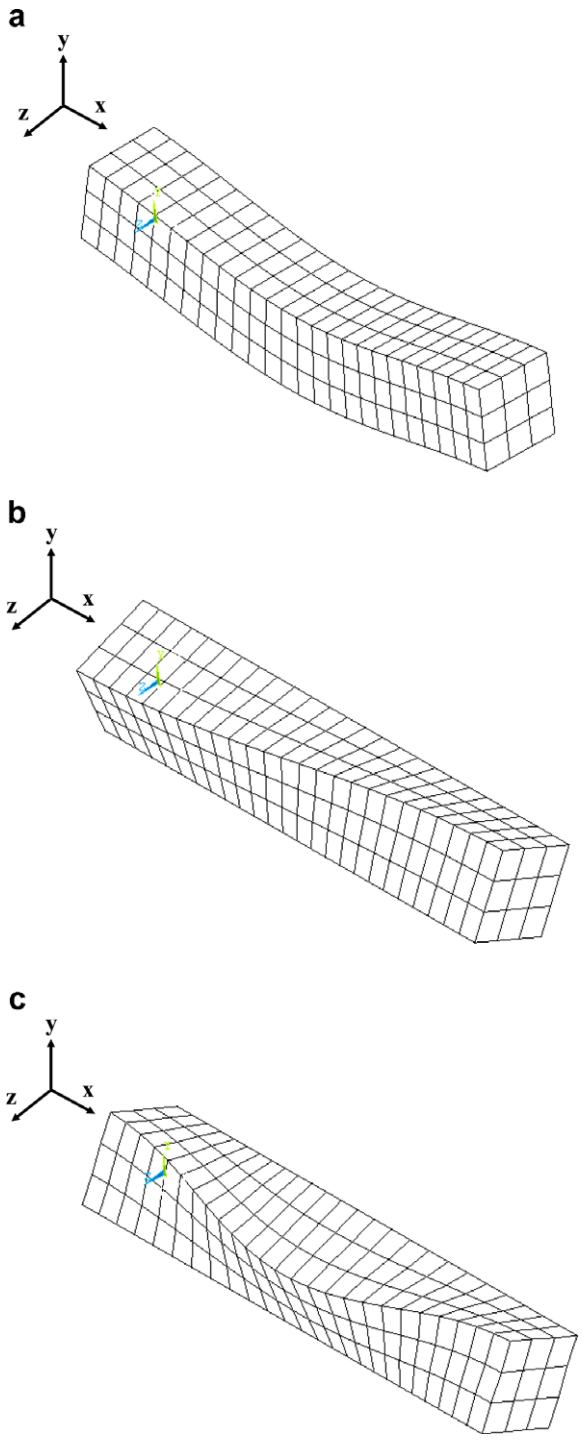

Fig. 9. The first three modal shapes of composite rod under free–free boundary conditions: (a) first mode; (b) second mode; (c) third mode.

Table 5
Fiber array effect on the first three modal damping capacities of composite rod under free–free boundary condition

	SEP	SDP	HP
First mode	0.02125	0.02245	0.02178
Second mode	0.01096	0.01330	0.01187
Third mode	0.02111	0.02228	0.02163

Table 6
Fiber array effect on the first three modal damping capacities of composite plate under free–free boundary condition

	SEP	SDP	HP
First mode	0.02097	0.02220	0.02150
Second mode	0.01378	0.01749	0.01543
Third mode	0.01821	0.02012	0.01911

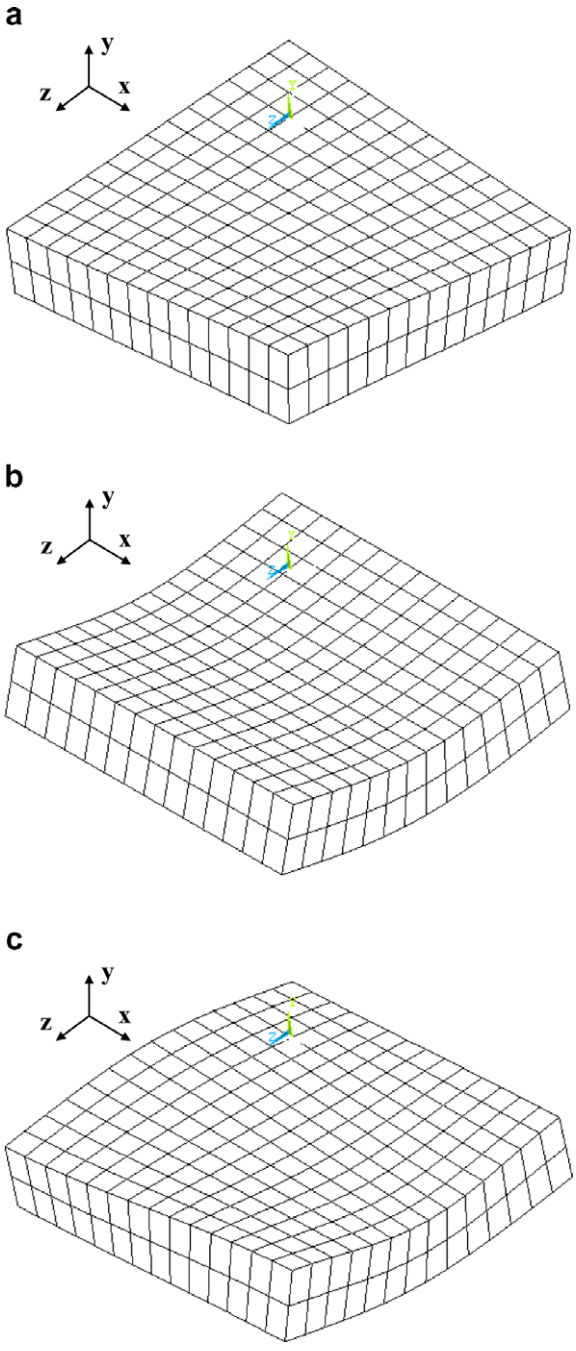

Fig. 10. The first three modal shapes of composite plate under free–free boundary conditions: (a) first mode; (b) second mode; (c) third mode.

damping capacities of the composite rod structures constructed based on three different fiber arrangements. Results reveal that the composites with SDP packing always exhibit a higher damping capacity than those with SEP and HP packings. Thus, it is suggested that during vibration, the composites with SDP microstructure were easier to dissipate strain energy.

The first three modal shapes for the composite plate with free–free boundary condition are shown in Fig. 10. Twisting in the *x*-direction is the first modal shape; the second one is the bending in the *x*-direction (fiber direction); and the third mode is the twist-

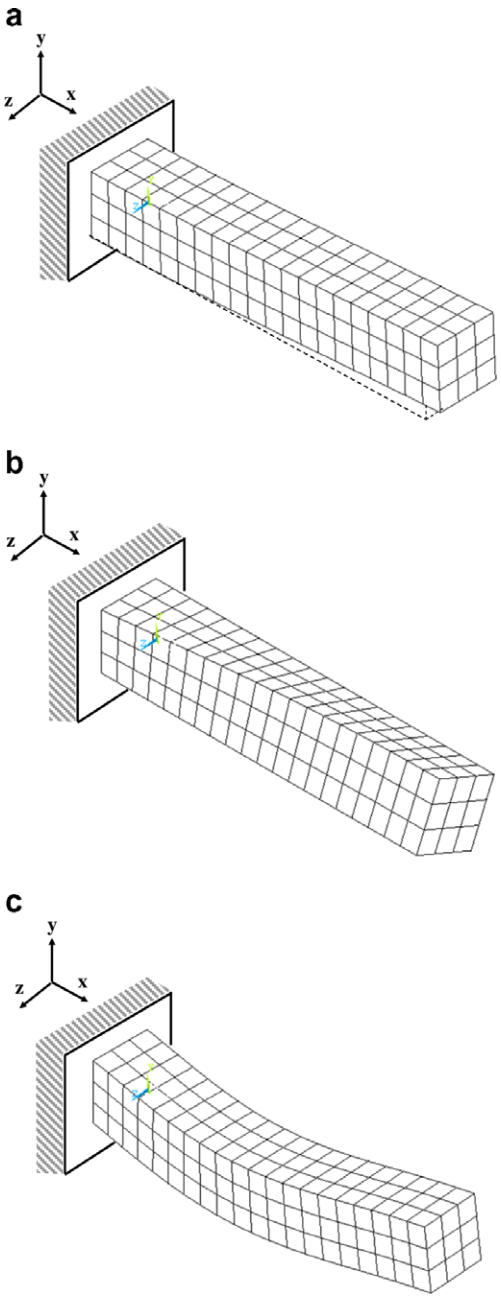

Fig. 11. The first three modal shapes of composite rod under clamp-free boundary condition: (a) first mode; (b) second mode; (c) third mode.

Table 7
Fiber array effect on the first three modal damping capacities of composite rod under clamp-free boundary condition

	SEP	SDP	HP
First mode	0.00699	0.00884	0.00767
Second mode	0.02115	0.02233	0.02167
Third mode	0.01433	0.01591	0.01499

Table 8
Fiber array effect on the first three modal damping capacities of composite plate under one side clamp boundary condition

	SEP	SDP	HP
First mode	0.00834	0.01046	0.00913
Second mode	0.01360	0.01478	0.01405
Third mode	0.01952	0.02099	0.02015

ing in the *z*-direction (transverse direction). The corresponding damping capacity for the modal shapes is shown in Table 6. Apparently, the composite plate constructed from SDP microstructure also possesses the highest damping capacity as compared to the other two cases. As a result, for the composite rod and plate in free vibration condition, the SDP fiber packing can provide the superior damping responses than the SEP and HP fiber arrays.

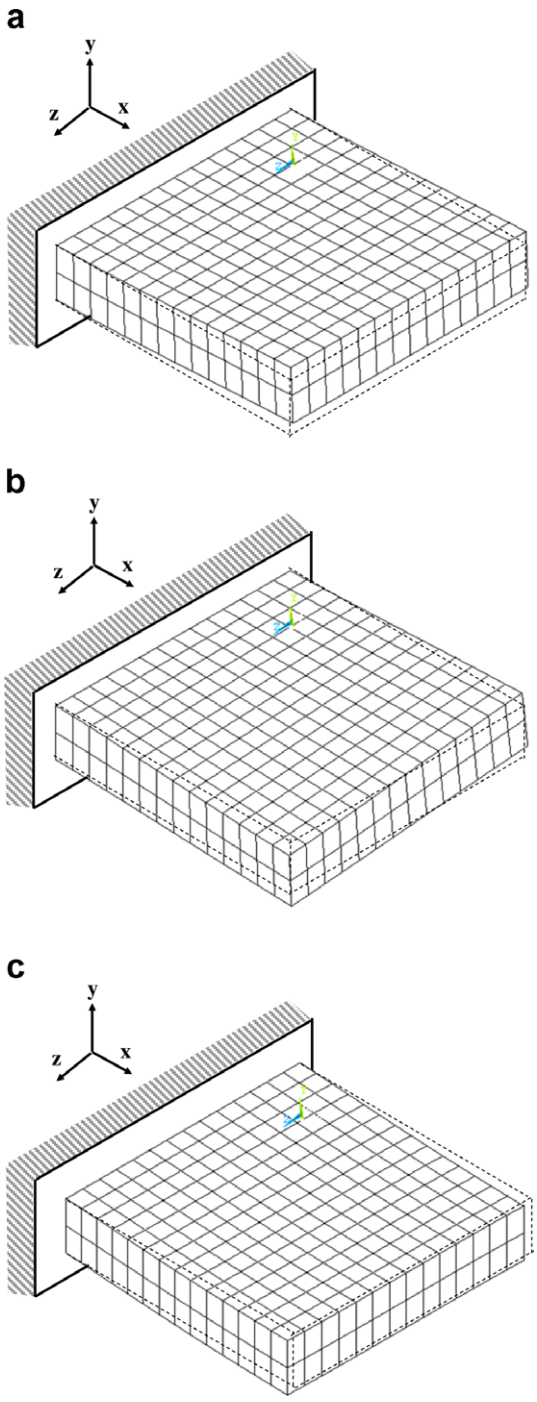

Fig. 12. The first three modal shapes of composite plate under one side clamped boundary condition: (a) first mode; (b) second mode; (c) third mode.

4.2. Vibration with clamped-free boundary condition

In addition to the free vibration, the cantilever type vibration, i.e., free-clamped boundary condition, was regarded in the study. The clamped end was always fixed in the *x*-direction. Fig. 11 illustrates the first three modal shapes of the composite rod. The first one and two modes are bending and torsion modes, respectively, and the third one is bending mode again. It is interesting to mention that the modal shapes of the unidirectional composites with clamped-free boundary condition are different from those in the free–free boundary condition. The corresponding damping capacities of the composite rods are listed in Table 7. Results show that SDP packing also demonstrates better damping capacity for the first three modes under cantilever type vibration.

Again, the plate type structure with one side clamp implemented in the *x*-direction was examined. The associated modal shapes were shown in Fig. 12. Moreover, the damping capacities for the composite plates were summarized in Table 8. Similar to the rod structure, the plate structure made of unidirectional composites with SDP fiber packing exhibits greater damping properties than the plates established based on the other two fiber arrays. In view of the forgoing investigations, it is suggested that the unidirectional composites created based on square diagonal fiber packing may be a better damping material as compared to the other composite materials.

5. Conclusions

The GMC micromechanical model was successfully extended to calculate the strain energy of the fiber composites with different fiber arrays, i.e., square edge packing, square diagonal packing, and hexagonal packing. Based on the energy dissipation concept, the damping capacity of the fiber composites in the material principal directions was determined. With the fundamental material properties, the modal damping capacity of the composites structures, i.e., composite rod and plate, constructed based on the three different fiber arrangements was calculated from the FEM analysis. Both free–free and free-clamp boundary conditions were considered in the analysis. Results indicate that the composite structures constructed based on square diagonal packing demonstrate superior vibration damping properties than the other two cases. From the investigation, it can be referenced by the composites material manufactures that with an appropriate design of the microstructures, the mechanical properties of fiber composites can be significantly modified.

Acknowledgement

This research was supported by the National Science Council, Taiwan, under the contract No. NSC 96-2628-E-009-009 to National Chiao Tung University.

References

[1] Zhu C, Sun CT. Micromechanical modeling of fiber composites under off-axis loading. J Thermoplast Compos 2003;16(4):333–44.

[2] Orozco CE, Pindera MJ. Plastic analysis of complex microstructure composites using the generalized method of cells. AIAA J 1999;37(4):482–8.

[3] Pindera MJ, Bednarcyk BA. An efficient implementation of the generalized method of cells for unidirectional, multi-phased composites with complex microstructures. Composites, Part B 1999;30(1):87–105.

[4] Tsai JL, Chi YK. Investigating thermal residual stress effect on mechanical behaviors of fiber composites with different fiber arrays. Composites, Part B 2008;39:714–21.

[5] Arnold SM, Pindera MJ, Wilt TE. Influence fiber architecture on the inelastic response of metal matrix composites. Int J Plasticity 1996;12(4): 507–45.

[6] Adams RD, Maheri MR. Dynamic flexural properties of anisotropic fibrous composite beams. Compos Sci Technol 1994;50(4):497–514.

[7] Berthelot J, Sefrani Y. Damping analysis of unidirectional glass and Kevlar fibre composites. Compos Sci Technol 2004;64(9):1261–78.

[8] Chandra R, Singh SP, Gupta K. Micromechanical damping models for fiber-reinforced composites: a comparative study. Composites, Part A 2002;33(6):787–96.

[9] He LH, Liu YL. Damping behavior of fibrous composites with viscous interface under longitudinal shear loads. Compos Sci Technol 2005;65(6): 855–60.

[10] Hwang SJ, Gibson RF. Prediction of fiber-matrix interphase effects on damping of composites using a micromechanical strain energy/finite element approach. Compos Eng 1993;3(10):975–84.

[11] Finegan IC, Gibson RF. Analytical modeling of damping at micromechanical level in polymer composites reinforced with coated fibers. Compos Sci Technol 2000;60(7):1077–84.

[12] Kaliske M, Rothert H. Damping characterization of unidirectional fiber reinforced polymer composites. Compos Eng 1995;5(5):551–67.

[13] Maheri MR, Adams RD. Finite element prediction of modal response of damped layered composite panels. Compos Sci Technol 1995;55:13–23.

[14] Drago A, Pindera MJ. Micro-macromechanical analysis of heterogeneous materials: macroscopically homogeneous vs periodic microstructures. Compos Sci Technol 2007;67(6):1243–63.

[15] Paley M, Aboudi J. Micromechanical analysis of composites by the generalized cells model. Mech Mater 1992;14(2):127–39.

[16] Ungar EE, Kerwin EM. Loss factors of viscoelastic systems in terms of strain energy. J Acoust Soc Am 1962;34(2):954–8.

[17] Hanselka H. Ein Beitrag Zur Charakterisierung Des Dämpfungsverhaltens Polymer Faserverbound-Werksofft. Dissertation, Technische Universität Clausthal, Germany, 1980.

[18] Gan H, Orozco CE, Herakovich CT. A strain-compatible method for micromechanical analysis of multi-phase composites. Int J Solids Struct 2000;37(37):5097–122.

[19] Cook RD, Malkus DS, Plesha ME. Concepts and applications of finite element analysis. New York: Wiley; 2002.